

Article

Impact of Climate Change on Combined Solar and Run-of-River Power in Northern Italy

Baptiste François ^{1,2,3,*} , Benoit Hingray ¹, Marco Borga ², Davide Zoccatelli ⁴, Casey Brown ³ and Jean-Dominique Creutin ¹

¹ Université de Grenoble-Alpes, CNRS, IGE, F-38000 Grenoble, France;

benoit.hingray@univ-grenoble-alpes.fr (B.H.); jean-dominique.creutin@univ-grenoble-alpes.fr (J.-D.C.)

² Department of Land, Environment, Agriculture and Forestry, University of Padova, IT-35020 Padova, Italy; marco.borga@unipd.it

³ Department of Civil and Environmental Engineering, University of Massachusetts Amherst, Amherst, MA 01003-9303, USA; casey@engin.umass.edu

⁴ Department of Geography, Hebrew University of Jerusalem, Jerusalem 9190401, Israel; davide.zoccatelli@mail.huji.ac.il

* Correspondence: bfrancois@umass.edu

Received: 5 December 2017; Accepted: 18 January 2018; Published: 25 January 2018

Abstract: Moving towards energy systems with high variable renewable energy shares requires a good understanding of the impacts of climate change on the energy penetration. To do so, most prior impact studies have considered climate projections available from Global Circulation Models (GCMs). Other studies apply sensitivity analyses on the climate variables that drive the system behavior to inform how much the system changes due to climate change. In the present work, we apply the Decision Scaling approach, a framework merging these two approaches, for analyzing a renewables-only scenario for the electric system of Northern Italy where the main renewable sources are solar and hydropower. Decision Scaling explores the system sensibility to a range of future plausible climate states. GCM projections are considered to estimate probabilities of the future climate states. We focus on the likely future energy mix within the region (25% of solar photovoltaic and 75% of hydropower). We also carry out a sensitivity analysis according to the storage capacity. The results show that run-of-the river power generation from this Alpine area is expected to increase although the average inflow decreases under climate change. They also show that the penetration rate is expected to increase for systems with storage capacity less than one month of average load and inversely for higher storage capacity.

Keywords: solar power; run-of-the river power; energy mix; Decision Scaling; climate change

1. Introduction

The United Nations Framework Convention on Climate Change (UNFCCC) 2015 Paris Agreement provides an ideal framework to move toward an energy transition from traditional to renewable energy sources. The agreement actually promotes the use of renewable energy sources instead of conventional energy sources (i.e., usually fossil ones). As discussed by Jacobson [1], the main fraction of power generation from renewable energy sources is expected to come from Variable Renewable Energy sources, hereafter noted as VRE (e.g., solar-, wind- and hydro-power). As highlighted by Engeland et al. [2], VRE power generation is characterized by a large degree of variability inherent to their driving climate variables (e.g., wind speed, precipitation, solar radiation, temperature . . .). The multiscale space-time variability of VRE complicates their integration into the electricity networks [3–5]. In any energy mix scenario with high shares of VRE, temporal variations of the production would not exactly match those of the load, leading to a succession of over- and under-production periods and, in turn to a risk

of not meeting the demand (e.g., [6]). The energy transition is even more complicated by the transitory climate conditions in which it should take places [7]. The evolution of the mean and time variability of weather variables remains uncertain, and thus the related impacts on VRE generation (e.g., [8] for solar Photovoltaic (PV)) and consumption (e.g., [9]) too. When setting energy transition pathways, the evolution of the society is also an important parameter to account for [10]. For instance local or national energy policies, promoting either solar-, wind- or hydro-power, might have various impacts in term of power generation, energy backup requirements and management (e.g., [11]).

Several studies investigate possible pathways of the European energy system toward a high share of renewable energies. Most of these studies give more consideration for the evolution of the infrastructures than for the change in VRE generation due to climate change. For instance, Becker et al. [12] analyze the potential evolution of the transmission lines that is required to allow integrating high share in solar and wind power generation, as expected by the European Union objectives. The evolution of the VRE sources due to climate change is in this case completely disregarded (i.e., the effects of climate change on solar radiation and wind speed (and thus on power generation) are not accounted for by Becker et al.).

The evolution of the VRE sources due to climate change is in this case completely disregarded (i.e., the effect of climate change on solar radiation and wind speed are accounted for by Becker et al., neither the resulting effect on power generation).

Some other studies focus on the impact of climate change on weather variables driving VRE power generation. These studies mainly rely on Global Circulation Models (GCMs). The GCM outputs are used as input into impact models such hydrological models, energy models or market models. If needed, intermediate regional downscaling models are used to adapt the GCM outputs to the scale of the considered system [13]. This analysis framework is often denoted as a top-down approach. For instance, Tobin et al. use such an approach for analyzing climate change impact on European wind power generation from the ENSEMBLES high-resolution climate projections [14] and from the EURO-CORDEX regional climate experiment [15]. Ref. [7] estimates changes in solar power generation in Europe from the EURO-CORDEX experiment. Climate change impacts on hydropower have been studied much earlier than for solar and wind power (e.g., [16,17]). As indicated in the review paper by Schaeffli [18], the top-down approach was mainly used in the hydropower literature for such an assessment (see [19] for an early reference).

However, Brown et al. [20] explain that it is often difficult to use the top-down approach for decision-making purposes because the results are only conditioned by the ensemble of considered future projections. As discussed in [21], the envelope of possible futures that is described by all available projections only provides a lower bound of the uncertainty of the 'real' envelope of possible futures. The sample of possible futures as seen by available GCM projections may thus underestimate the change in performance of any systems [22]. Other drawbacks that limit the use of top-down approach for decision-making is that no probability can be attached to GCM projections and that two GCM projections can predict two evolutions of the system that are significantly different (see the discussion of this topic by Kundzewicz and Stakhiv [23]).

An alternative approach, denoted as 'bottom-up' starts from an understanding of the dependencies between the performance or vulnerability of the considered system and its climatic drivers. This understanding usually follows from the stochastic exploration of plausible climate states, which may reveal thresholds, tipping points and other vulnerabilities as well as opportunities. One can thus note that bottom-up approaches depart from conventional top-down approaches because they explore the sensitivity of the system response to a plausible range of climate states rather than exploring its sensitivity to the temporal sequences of weather variables that are obtained out of each available GCM projection. Whether the bottom-up approach increases the understanding of the considered system, especially its changes in performance/vulnerability should the climate changes; this approach does not inform on the future evolution of the system.

In this study, we use Decision Scaling, an approach that merges top-down and bottom-up approaches. Decision Scaling is based on the scenario neutral approach [24]. It was originally designed for testing the robustness of water systems (see [20,25,26] for recent applications). Decision Scaling is specifically designed to address the shortcomings of GCM projections use at project scales. It mainly relies on the development of Climate Response Functions (CRFs). For any considered system, a CRF shows the link between a chosen indicator of the system's performance and different climate states (e.g., different annual averages of weather variables driving the VRE power generation). In a second stage, Decision Scaling uses the ex post GCM projections to infer about the plausibility of the future climate states leading to change in system's performance as observed on the CRF.

We use Decision Scaling for analyzing a 100% renewable energy system covering three provinces in the North-Eastern Italy (Figure 1). Solar and hydro-power are the main VRE sources in this region (with a high share of run-of-the river (RoR) hydropower). The considered performance indicator is the 'energy penetration' rate, which is defined as the long-run percentage of energy demand that is directly met by the VRE on an hourly basis. The CRFs are developed in a 2D climate change space (annual change in mean precipitation and temperature). They are obtained from multiple time series of precipitation and temperature that are obtained by perturbing the observed weather time series following the change factor method.

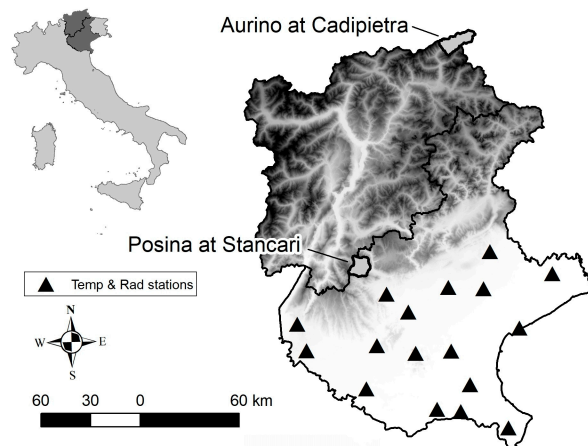


Figure 1. Topographic map of the study region in Northern Italy. The catchments of Aurino at Cadipietra (149.8 km²) and Posina at Stancari (116 km²) are shown by light gray areas. Along the climate transect from the alpine crests to the Veneto plain (dry and snowmelt dominated at high elevations and wet and precipitation dominated at lower elevations), these two catchments represent a benchmark of the opposite locations of hydropower plants in this region. Location of solar irradiance and temperature measurements in the Veneto plain area are indicated by black pyramids.

Climate change projections from the ex-post GCM projections from the Climate Model Intercomparison Project phase 5 (CMIP5) are further used for assessing these change factors for the Representative Concentration Pathway 8.5 and for different climate models and different future prediction lead times. Future system performance/vulnerability to climate change is then discussed by putting in perspective the CRF and the change factor as obtained from GCM projections. As mentioned above, this also allows inferring probabilities of future climate states and thus probabilities of system performance changes.

Although all possible combinations between solar PV and RoR hydropower might be considered, we mainly focus on the 25% solar 75% hydro mix, which is the most likely future energy mix in the studied area.

The study is organized as follows: Section 2 describes the study area. The database and the models are presented in Section 3. Section 4 show the results obtained for the control climate. The results

obtained through the Decision Scaling approach are presented in Section 5. The Section 6 concludes and gives some outlooks for future works.

2. Study Area

The area selected in North-Eastern Italy includes three main administrative units: Regione Veneto, Provincia Autonoma di Trento, Provincia Autonoma di Bolzano-Southern Tyrol. The area crosses part of the Alps with a climatic gradient from essentially snow-fed catchments at the Northern edge to rainfall fed catchments at the Southern edge of the transect [27]. The regional administrative units coordinated their energy policy, optimizing the joint use of the main renewable energy sources, namely solar and hydropower (see C3-Alps project <http://www.c3alps.eu/>).

A number of hydropower stations have been operational for decades in the region. They are operated by public institutions, private companies or consortia of municipalities and local communities. Hydropower production is characterized by a high share of RoR power generation, as in the rest of the country where RoR generation reached almost 43% of the hydropower generation in 2011 (for a power capacity equal to 27% of the total hydropower capacity) [28].

Veneto province is the second largest producer of PV power in the North of Italy. In 2011, the regional PV power capacity reached more than 370 MW with a surface more than 18 km² covered by PV systems. This power capacity is share between big PV farms, such as the one located in Rovigo (with 70 MW of installed capacity, this farm is the largest in the area), and private PV systems located on building roofs. In the recent years, a number of private initiatives were proposed for developing PV production in the area. An illustration is the deployment of demo floating PV systems on artificial reservoirs and water ponds (irrigation reservoirs, drinking water reservoirs, . . .) by the Institute for Renewable Energy of the European Academy of Bolzano [29].

3. Data and Methods

The flow diagram on Figure 2 summarizes the analysis framework. Each component of the analysis framework is described below, including the database, the hydrological model, the energy and load modeling and the different climate scenarios used to build the CRFs. By carrying out simulations at an hourly time step, we may account for the three key cycles of the load and generation fluctuation—daily, weekly and seasonal. The time step series are obtained over the 1992–2010 period.

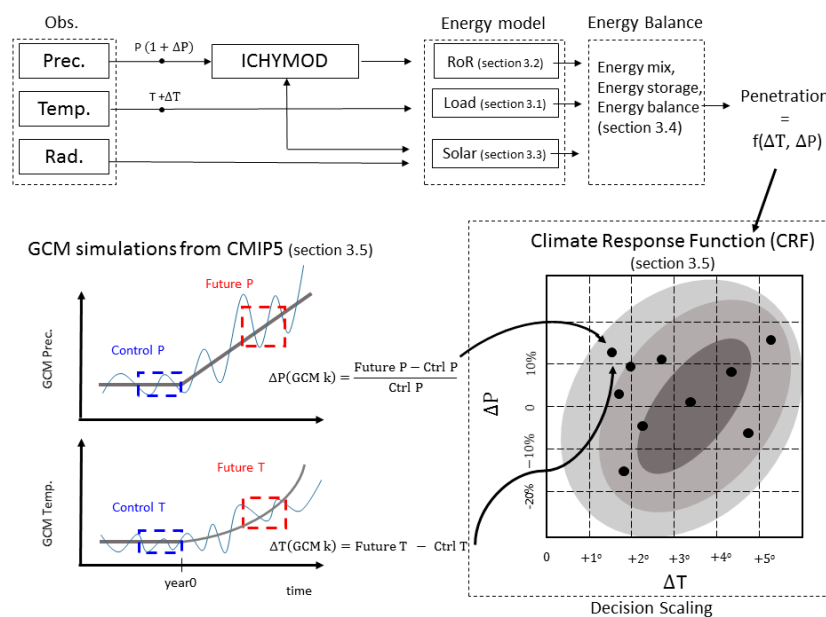


Figure 2. Flow diagram of the analysis framework.

3.1. Regional Energy Load

No time series of electricity consumption is available for the Veneto, Trento and Bolzano-Southern Tyrol provinces. We therefore estimate the regional electricity consumption by weighting the time series of the national consumption according to the Gross Domestic Product (GDP) of these three provinces, which roughly represented 8% of the Italian GDP in 2013. The electricity consumption data for Italy were provided by the European Network of Transmission System Operators of electricity (<https://www.entsoe.eu/home/>). The hourly database is available from 2006 to 2013. The Italian average hourly consumption equals 38 GWh, leading to an estimate of 3 GWh for the three provinces.

As illustrated by François et al. [30], economic and societal features affect daily, weekly and annual patterns of electricity demand with high consumption peaks around noon and during the evening and low consumption sequences during weekends, holiday periods and civil or religious celebrations. In addition to these human drivers, the air temperature also influences the electricity consumption. The so-called Temperature Dependence Pattern [31] in Italy presents increased consumption during hot and cold days, related to energy needs for cooling and heating systems respectively.

The weather variables that drive both hydropower and solar PV generation are available from 1992. A daily electricity consumption model has been developed by François et al. [30] in order to extend the analyzed period prior to the year 2006. Daily electricity consumption is estimated based on the heating and cooling degree-day method [32] by the following piecewise linear relation:

$$\begin{cases} L(t) = a_{i,j,T_{Heat}} \times [T_{Heat} - T(t)] + b_{i,j} \text{ if } T(t) < T_{Heat} \\ L(t) = b_{i,j} \text{ if } T_{Heat} < T(t) < T_{Cool} \\ L(t) = a_{i,j,T_{Cool}} \times [T(t) - T_{Cool}] + b_{i,j} \text{ if } T(t) > T_{Cool} \end{cases} \quad (1)$$

where L is the simulated energy load for the day t , T is the daily temperature, i and j are dummy variables expressing the day of the week (i.e., weekday, Saturday or Sunday), and the period (i.e., holiday or not). In between temperature thresholds T_{Cool} and T_{Heat} , the air temperature is assumed as having no influence of the energy load. Higher electricity consumption are simulated for air temperatures higher than T_{Cool} or lower than T_{Heat} (i.e., $a_{i,j,T_{Heat}} < 0$ and $a_{i,j,T_{Cool}} > 0$). This model allows estimating for long temporal periods the day-to-day variations of the load due to temperature variations.

The sub-daily variations of the load are obtained with the non-parametric disaggregation method developed by François et al. [30]. For each simulation day, it uses the observed sub-daily anomaly pattern of a day randomly selected from days of the same calendar period (e.g., 30-day calendar interval centered on the simulation day). The prediction skill of this energy load model is quite high, accordingly with the Nash-Sutcliffe efficiency [33], which ranges from 1 (perfect model) to minus infinite. Nash-Sutcliffe efficiency values obtained for calibration and evaluation periods (2006–2009 and 2010–2012) are equal to 0.85 and 0.79, respectively.

3.2. Run-of-River Hydropower

By choice in our study, we consider the run-of-river (RoR) hydropower generated from the natural river flow, i.e., without dam control along rivers. The power at a given time t is thus generated from the water discharges of a selected catchment:

$$p(t) = \eta_H g h \rho q(t) \quad (2)$$

where p is the power delivered by a generator (kW), η_H the efficiency of the generator (no units), q the water flow through the turbines ($\text{m}^3 \text{s}^{-1}$), g the acceleration of gravity ($\text{m}^3 \text{s}^{-2}$), ρ the water density (kg m^{-3}) and h the falling height (m). For a given plant, the power generation is classically bounded by three characteristic flows corresponding to technical and environmental constraints. In the present case, no hydropower is produced if the river discharge is lower than the minimum discharge value

Q_{min} required to fulfill downstream environmental requirements (i.e., the lowest acceptable flow in the natural river network). The production is also interrupted to prevent any potential damages to the power plant when the discharge exceeds the safety threshold Q_{max} . The plant design flow Q_d finally determines the maximum river discharge that can be diverted to the power plant. In this study, values of Q_{min} , Q_{max} and Q_d , are constant in time and fixed equal to the 95th, 2nd and 25th percentiles of the natural flows; as discussed by Hänggi and Weingartner [34], these values are usual for RoR power plants. These thresholds are estimated for the 1992–2010 period and remain unchanged for the whole analysis.

We consider two different hydro-climatic regions from where RoR power is generated (Figure 1). We selected one catchment from each region with the typical size of the catchment equipped with run-of-the-river power plants in the region: Aurino at Cadipietra (149.8 km²) and Posina at Stancari (116 km²). They are located at the opposite bounds of the climatic gradient mentioned previously. Aurino is mainly a snow-dominated catchment, whereas Posina is mainly a rainfall fed catchment. Both catchments are not significantly influenced by dams or significant diversions. We assume that the selected catchments are good indicators of the temporal organizations of the production of similar power plants distributed within the same hydro-climatic region.

The Integrated Catchment Hydrological Model (ICHYMOD) was used for simulating water discharge time series from weather data for both Aurino at Cadipietra and Posina at Stancari catchments [35,36]. This conceptual and semi-distributed model simulates at hourly time steps the processes of snow accumulation and ablation, evapotranspiration and soil humidity. The snow accumulation and ablation module is based on hourly temperature combined with a distributed radiation index, based on local morphology [37]. Potential evapotranspiration is calculated based on regional maximum and minimum temperatures [38]. The soil partition of precipitation into evapotranspiration, surface and subsurface flow components is regulated through the Probability Distributed Model [39]. ICHYMOD was calibrated and validated over Aurino at Cadipietra and Posina at Stancari catchments over the period 1990–2000 and 2001–2010, respectively (with Nash-Sutcliffe efficiency values equal to 0.83 and 0.76 for Aurino and for the calibration and validation periods; and 0.82 for both periods for Posina at Stancari). Hourly observed precipitation, temperature and discharge data bases were provided by the regional environmental agencies. Simulated water discharges are then used for computing RoR power generation at the outlet of both catchments (Figure 2).

For the alpine region, i.e., the Aurino at Cadipietra catchment, discharges are mainly governed by the dynamics of the snowpack (accumulation and melt). The resulting power generation presents significant seasonal signal with low generation during winter and high generation during spring floods (Figure 3a). For the lowland region, i.e., Posina at Stancari catchment, the temporal structure of power generation follows the seasonality of rainfall amounts that are higher in early spring and during the fall season (Figure 3a). In both climatic areas, no significant diurnal cycle is observed (Figure 3b).

3.3. Solar PV Power Generation

Solar photovoltaic (PV) power generation from a horizontal photovoltaic generator (P_{PV}) is computed at 17 locations where hourly air temperatures T_a (°C) and global solar irradiance I_{eff} (Wm⁻²) are available in the Veneto plains (black pyramids in Figure 1). Observed hourly temperature and solar radiation data are provided by the Regional Agency for the Prevention and Environmental Protection of the Venetian (ARPAV) for the 1992–2010 period. Missing data (less than 2% of the time series) were reconstructed from the nearest station. We assume that the total power generation obtained from equally weighting the 17 available local power generation series is representative of a regional PV system.

At a given time t , power generation can be estimated as a function of the measured global solar irradiance I_{eff} (Wm⁻²) and air temperature T_a through the following expression [40]:

$$P_{PV}(t) = B \times I_{eff}(t) \times \left(1 - \mu(T_a(t) - T_{c,STC}) - \mu \cdot C \cdot I_{eff}(t)\right), \quad (3)$$

where μ and C are parameters controlling the conversion efficiency according to the air temperature and the radiation. B is a constant production parameter equal to the product of the inverter efficiency (conversion from direct to alternative current) by the surface area of the PV array and the generator efficiency under the standard test conditions, defined by a cell temperature $T_{c,STC}$ equal to 25 °C and a solar irradiance I_{STC} equal to 1000 Wm⁻² [41]. In the study area, solar PV power generation follows the diurnal and seasonal variations of radiation and temperature with high values around noon and summer (Figure 3).

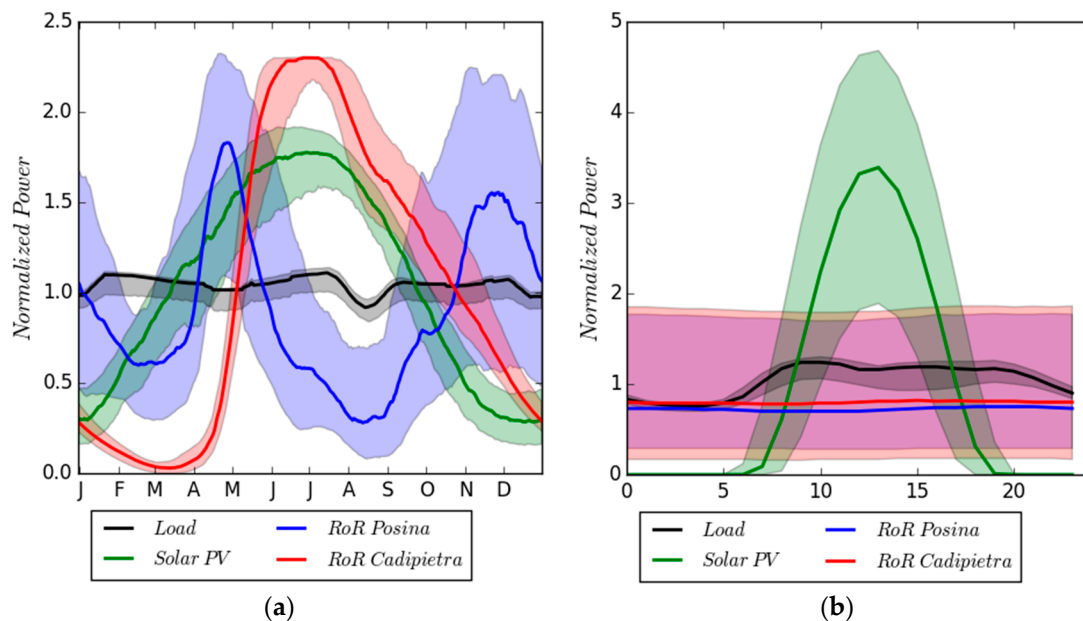


Figure 3. Annual (a) and daily (b) average cycles of simulated energy load (black) and simulated energy generation (i.e., solar PV generation (green) and RoR power generation from the snow- (red) and rain-dominated (blue) catchments and for the present climate (1992–2009). Bold curves represent the median cycle while shaded areas show distance between 25th and 75th percentiles. The time step used is hourly for daily cycles and daily for annual cycles (For illustration, all the cycles have been normalized to their average value. Hence, the average value of the cycles equals 1).

3.4. Evaluating the Penetration Rates of VRE Mixes

For this study, the region is considered as autonomous in a sense that there is no energy import/export with neighboring regions. The regional electricity consumption can be only satisfied (or not) with the production obtained within the region from solar and RoR power generation. Furthermore, the study area is regarded as a ‘copper plate’ grid, meaning that the energy can circulate instantaneously within the region without energy losses. This assumption has been used for systems with spatial scales ranging from local (e.g., [42]), to regional (e.g., [6,30,43,44]), country (e.g., [45] for Germany and [46] for UK) and continental (e.g., [47–49] for the European continent). Although this assumption may appear crude for analyzing real systems, the context of our study is different. We aim at analyzing how complementarity between small run-of-the river hydro power plants and solar power may change under climate change for a region in Northern Italy. While several studies analyze the how climate change affects single renewable energy source (e.g., [7,14,15,17,50]), studies that look at how climate change affects the complementarity among different energy sources are rather limited. This study contributes to this effort. In that context, the copper plate assumption provides an ideal platform for analyzing the complementarity among energy sources resulting from their natural availability and variability both in space and time. The complementarity among energy sources also depends on system constraints (such as the electricity grid) and those constraints will also evolve in the future as a result of system development and adaptations. We however believe that the first order

drivers of the complementarity are the variability and the co-variability features of hydro-climatic drivers. We also believe that focusing on those drivers gives important and meaningful information for the complementarity that may be achieved for different technical configurations of the power system. As these features are likely to change with climate change, characterizing these changes is also potentially helpful for a relevant planning of future adaptations/developments of electricity systems.

RoR and solar PV power generation time series are scaled so that the regional electricity consumption is on average satisfied over the considered period. This configuration is often denoted as 100% renewable scenario). Such configuration is obtained by dividing each time series by their average and then multiplying by the consumption average:

$$P(t) = \frac{p(t)}{\langle p(t) \rangle} \langle L(t) \rangle \quad (4)$$

with p the energy generation from one energy source in a given region (Wh), L the in situ energy load (Wh) and P the scaled energy production (Wh). $\langle x \rangle$ is the temporal mean of x . The average production from the energy mix thus equals the average of the simulated electricity consumption over the whole period 1992–2010 (i.e., 3 GWh per hour on average).

A mixed run-of-the-river power generation from the two hydro-climatic regions is given by:

$$P_H = S_H P_{H_{Snow}} + (1 - S_H) P_{H_{Rain}} \quad (5)$$

where $P_{H_{Snow}}$ and $P_{H_{Rain}}$ are the scaled hydropower generation from RoR plants located on snowmelt and rainfall dominated regions, respectively, and S_H the sharing coefficient between the two hydro-climatic areas ($0 < S_H < 1$). When $S_H = 1$, the hydropower generation comes from the alpine area only and when $S_H = 0$, the hydropower generation comes from the downstream area only.

Mixed power generation scenarios are obtained by coupling PV and RoR power generation using a sharing coefficient denoted S_{PV} :

$$P_{Mix} = S_{PV} P_{PV} + (1 - S_{PV}) P_H \quad (6)$$

where P_{Mix} is the power generation from the energy mix. S_{PV} equals 1 when the whole generation comes from PV systems, and inversely, S_{PV} equals 0 when the whole generation comes from hydropower. Including expression P_H in Equation (6), we obtain:

$$P_{Mix} = S_{PV} P_{PV} + (1 - S_{PV}) (S_H P_{H_{Snow}} + (1 - S_H) P_{H_{Rain}}) \quad (7)$$

Note that when S_{PV} equals 1, S_H value does not matter. Note also that the energy mix corresponding to an equal distribution of production between the three considered energy sources would be obtained with $S_H = 0.5$ and $S_{PV} = 0.33$. Even though it is not yet really clear what will the energy mix look like in the next decades, the scenario corresponding to 25% of generation coming from solar PV systems and 75% of hydropower seems to be a good guess within the studied area (i.e., $S_{PV} = 0.25$). A high share of hydropower coming from the mountainous areas is also expected (i.e., $S_H = 0.75$). We mainly focus on this scenario.

We also consider the possibility to use some energy storage facilities to store energy in case of energy production excess and to release energy during periods of insufficient VRE production. We assume that both solar PV and RoR power generation can be stored and released with the same power efficiency. For instance, this might be achieved using batteries or pumped hydro storage technologies. In such a case, the energy storage time fluctuation is given by:

$$S(t+1) = \begin{cases} \min[S^{max}, S(t) + \eta_{in}\Delta(t)], & \text{if } \Delta(t) > 0 \\ \max[S^{min}, S(t) + \eta_{out}\Delta(t)], & \text{if } \Delta(t) < 0 \end{cases} \quad (8)$$

where $\Delta(t)$ is the hourly energy balance defined as the time difference between hourly generation and consumption, $S(t)$ is the actual storage varying between a minimum value S^{min} (set to 0 here) and the maximum storage capacity of the system (S^{max}) and where η_{in} and η_{out} are respectively the storage and power generation efficiencies. In this system, any energy production excess is lost when the actual storage reaches the storage capacity limit.

In the following, we will consider different system configurations with storage capacities S^{max} ranging from one hour to six months of average load. The range of solutions that could provide such storage capacities depends obviously on the considered region and its grid structure. Beaudin et al., [51] reviewed current storage solutions and show that a combination of several technologies is needed to balance the different variability features of VRE generation. Batteries could for instance be used for grid stability, pumped storage for load following, and flow batteries and compressed air energy storage for seasonal storage. Even though each storage technology presents its own constraints and efficiency, for the sake of simplicity we assume a perfect efficiency for all considered storage capacities ($\eta_{in} = \eta_{out} = 1$). Broadly speaking, we explore how smoothing the range of sub-daily to monthly variability of a given production with increasing storage capacity affects the rate of load satisfaction. In order to compare in a consistent way the simulation results obtained with the different storage capacity scenarios, the initial value of the actual storage is always set to 0.

The penetration rate PE (%) is defined as the percentage of the energy load that is supplied during the studied period. It is estimated from the hourly time series. The penetration indicator was used in previous studies for characterizing how power generation from a mix of renewable energy sources matches the demand (e.g., [6,43,52,53]).

3.5. Future Scenarios

Within the Decision Scaling analysis framework, we focus on changes in mean annual precipitation and temperature that are the two main climatic drivers of change for energy load and RoR power generation via changes in hydrological regimes. CRFs are thus expressed in a two dimensional climate change space and built from multiple hydro-climatic time series. To build the CRFs illustrated on the flow diagram on Figure 2, and then later in Section 5, we simply apply absolute (respectively relative) change factors to the observed temperature (respectively precipitation) time series. The change factors range from -50% to $+50\%$ with a 10% step for precipitation (ΔP) and from 0 to $+8$ °C with $+1$ °C step for temperature (ΔT). This yields to 98 bivariate scenarios plus one status-quo scenario. The resulting time series of precipitation and temperature are then used as input of hydrological model, electricity consumption model and energy generation model. Note that change factors considered for producing the CRFs are not obtained from the GCM projections. They are chosen to uniformly sample all possible scenarios of change (i.e., the space that defines all possible combination of temperature and precipitation changes).

Positioning on the CRFs future projections of GCM experiments allows discussing the credibility of the VRE penetration obtained for the considered climate states (see black dots on the CRF in Figure 2 and colored dots in the CRFs in Section 5). In the present case, we consider future projections of a multi-model ensemble of CMIP5 GCMs experiments [54]. In recent climate change studies, change factors are classically obtained from the change between a future and a reference period obtained from the raw climate model outputs (e.g., absolute for temperature or relative for precipitation). Such estimation of change factors is sensitive to low-frequency variations, commonly termed as climate internal variability. Low-frequency variability can either temporally decrease or increase the perception of long-term climate change (or even reverse its sign). Consequently, change factors classically estimated from raw climate projections are likely to misestimate change factors that are expected from the noise-free climate signal (the uncertainty coming from the internal variability has actually been found to be a major limitation for a robust estimation of change factors, especially for precipitation variables as discussed in [55,56]). In this work, we estimate the climate change factors for each GCM projection by using all data of the transient simulations available for the model (150 years

from 1950–2099). For each GCM projection, we first fit a trend model to the raw climate projections following Hingray and Said [57]. A piece-wise linear function of time is considered for precipitation and a third order polynomial trend is used for temperature. We then compute the change factors from the trends (Figure 2).

This approach was applied to estimate the change factors for 25 climate models, one representative concentration pathway (i.e., the Representative Concentration Pathways 8.5), and three prediction lead times, namely 2040–2059, 2060–2079 and 2080–2099 (Table 1). Data and detailed description of the models are available at the CMIP5 archive (<https://esgf-node.llnl.gov/search/cmip5/>). These GCMs were chosen according to their data availability at the time this study was conducted. Note that some of the considered climate projections may not be independent because obtained from models that are developed (partially or totally) within the same institutes. Accounting for the effect of GCM similarities is out of the scope of our study. The reader is invited to head to Refs. [58,59] for broader discussion about the how GCM projection similarities affect the climate change assessment. The reference period is 1992–2010. As illustrated on Figure 4, the temperature is expected to increase with time although the model uncertainty is rather large over the studied area. The deviation between minimum and maximum temperature changes roughly equals 2.5 °C for the 2040–2059 period and more than 4 °C for the 2080–2099 period. Model uncertainty for precipitation changes is very large and even the sign of change is uncertain. The grand ensemble mean tends to decrease but for some GCMs an increase of precipitation is indicated.

Table 1. GCM model considered from CMIP5 experiment. All considered projections are obtained for the Representative Concentration Pathways 8.5.

Modeling Center	Model	Institution
BCC	BCC-CSM1.1 BCC-CSM1.1(m)	Beijing Climate Center, China Meteorological Administration
CCCma	CanESM2	Canadian Center for Climate Modelling and Analysis
CMCC	CMCC-CM	Centro Euro-Mediterraneo per I Cambiamenti Climatici
CNRM-CERFACS	CNRM-CM5	Centre National de Recherches Météorologiques ; Centre Européen de Recherche et Formation Avancées en Calcul Scientifique
CSIRO-BOM	ACCESS1.0	CSIRO (Commonwealth Scientific and Industrial Research Organisation, Australia); BOM (Bureau of Meteorology)
CSIRO-QCCCE	CSIRO-Mk3.6.0	Commonwealth Scientific and Industrial Research Organisation in collaboration with the Queensland Climate Change Center of Excellence
GCESS	BNU-ESM	College of Global Change and Earth System Science, Beijing Normal University
INM	INM-CM4	Institute for Numerical Mathematics
IPSL	IPSL-CM5A-MR	Institut Pierre-Simon Laplace
LASG-CESS	FGOALS-g2	LASG, Institute of Atmospheric Physics, Chinese Academy of Sciences, and CESS, Tsinghua University
MIROC	MIROC5 MIROC-ESM MIROC-ESM-CHEM	Atmosphere and Ocean Research Institute (Univ. Tokyo); National Institute for Environmental Studies; Japan Agency for Marine-Earth-Science and Technology
MPI-M	MPI-ESM-MR	Max Planck Institute for Meteorology (MPI-M)
MRI	MRI-CGCM3	Meteorological Research Institute
NSA GISS	GISS-E2-R	NASA Goddard Institute for Space Studies
NCAR	CCSM4	National Center for Atmospheric Research
NCC	NorESM1-M	Norwegian Climate Center
NOAA GFDL	GFDL-CM3 GFDL-ESM2G GFDL-ESM2M	Geophysical Fluid Dynamics Laboratory
NSF-DOE-NCAR	CESM1(BGC) CESM1(CAM5)	National Science Foundation; Department of Energy; National Center for Atmospheric Research

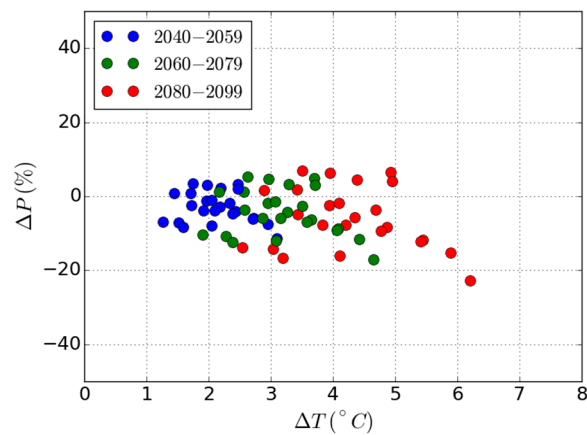


Figure 4. Scatter plot of changes in mean annual precipitation and temperature expected between a control period (1992–2010) and three future periods (i.e., 2040–2059; 2060–2079; 2080–2099) for 25 CMIP5 GCM experiments.

4. Penetration Rates for the Current Climate (1992–2009)

This section presents the penetration rates obtained over the control period (1992–2010) for each single source and for the likely energy mix for the next decades (i.e., $S_{PV} = 0.25$ and $S_H = 0.75$). The absolute shares of PV, alpine RoR and lowland RoR are thus respectively 25%, 56% and 19%. Following the analysis framework defined by the Equation (4), we use a 100% VRE scenario meaning that the average generation equals the average consumption over the considered period.

Figure 5 shows the penetration rates obtained for the control period and different storage capacities. Without any storage facility, the diurnal variability of solar power generation (see Figure 3b) makes its penetration rate rather low (i.e., about 42%). The solar penetration increases by about 30% moving from a no-storage to a twelve-hour storage configuration and by 25% more when the storage is further raised to three months. Increasing the storage capacity to six months has almost no further effect.

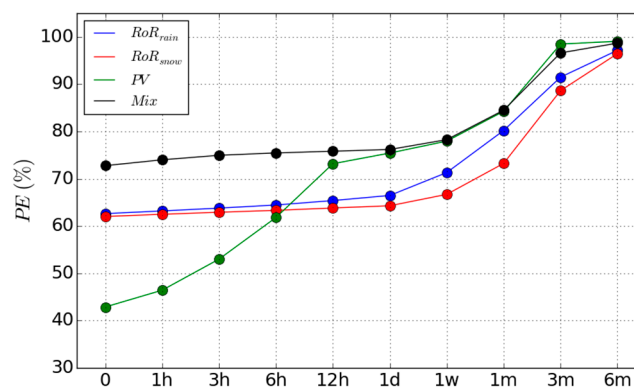


Figure 5. Evolution of the penetration rates with the storage capacity for solar PV power (green), RoR power coming from either snowmelt dominated (red) or rain-fed (blue) catchments and for the mix defined by $S_{PV} = 0.25$ and $S_H = 0.75$ (black). Values of storage capacities are given in hours of average load; h , d and m respectively mean hour, day and month.

Without storage, RoR penetration rates for either rain-fed or snowmelt dominated regions are roughly equal (62.6 and 61% respectively). They do not significantly increase when raising up to 24 h of storage (+3.9% and +2.3%, respectively) as expected from the low sub-daily discharge variability illustrated in Figure 3b. Catchment low-pass filter smooths the variability of rainfall and snowmelt both

in time due to the internal basin storages and in space with the branching structure of the hydrological network. This rather high temporal persistency makes RoR power generation often higher or lower than the load during sequences of days. RoR penetration rates significantly increase when going from one week of storage, roughly corresponding to the characteristic persistence of weather configurations, to three months of storage partly coping for discharge seasonality (+25.9 and +30.4% respectively).

Figure 5 also highlights the advantage of combining the considered energy sources. Without storage, the penetration rate of the mix is respectively higher than RoR power and solar PV by about 10% and 30%. The penetration of the mix gradually improves by only 4.2% when raising the storage capacity up to one week. Further, lifting the storage up to a capacity of the trimester demand clearly improves the penetration by over 20%.

5. Penetration Rates for Future Climates

This section presents first the possible impacts of climate change on load, RoR and solar PV power generation, as estimated via the Decision Scaling approach as described in Section 3. The resulting change in penetration rate is further discussed for the considered storage capacities.

5.1. Future Electricity Consumption, RoR and Solar PV Power Production

Figures 6 and 7 illustrate, for Posina and Cadipietra catchments respectively, the annual and seasonal changes in water discharges and RoR power generation for a selection of precipitation and temperature change scenarios.

At both locations, change in precipitation appears to be the main driver of changes in river flows with a roughly linear relationship between the average changes in precipitation and discharge. Due to the considered technical and environmental constraints of hydropower generation (see Section 3.2), an increase in water discharges may turn into either a decrease or an increase in RoR power generation during some periods. For instance, the RoR generation from Cadipietra catchment collapses during the late spring season for large precipitation increases (Figure 7d). This follows from longer and/or more frequent sequences where water discharges exceed the safety threshold Q_{max} leading to longer and/or more numerous power plant curtailments. Besides these threshold effects, RoR power generation seasonality remains almost unchanged when considering precipitation changes only.

Changes in temperature have different impacts in the two considered climatic areas. The evaporation effect reflected is slightly more important in low land than in altitude and leads to lower water discharges with higher temperatures (see the shape of the CRFs Figures 6e and 7e).

For the lowland Posina catchment, all the considered GCMs indicate a decrease of average water discharges, which turns into a decrease of average RoR power generation (Figure 6e,f). For the alpine Cadipietra catchment, the RoR generation evolves in a more unexpected way. Most GCMs indicate a decrease in average discharge and an increase in average RoR generation. This results from the role of temperature in alpine regions. In such areas, a warmer climate implies that more precipitation falls as rain instead of snow. The hydrological behavior of the catchment turns to be rainfall dominated. Less snow accumulation results to higher water discharges during autumn and winter seasons and lower water discharges during the spring flood season. Higher winter/autumn discharges are more frequently greater than the environmental flow threshold Q_{min} , permitting many additional winter days of RoR production. Lower spring discharges are more frequently below the safety threshold Q_{max} , limiting power plant curtailments. Both threshold mechanisms smooth the RoR generation during the year. RoR generation decreases only when this threshold effect does not make up for the decrease in discharges. This is for instance the case for the GCMs predicting a decrease in average precipitation higher than 12%.

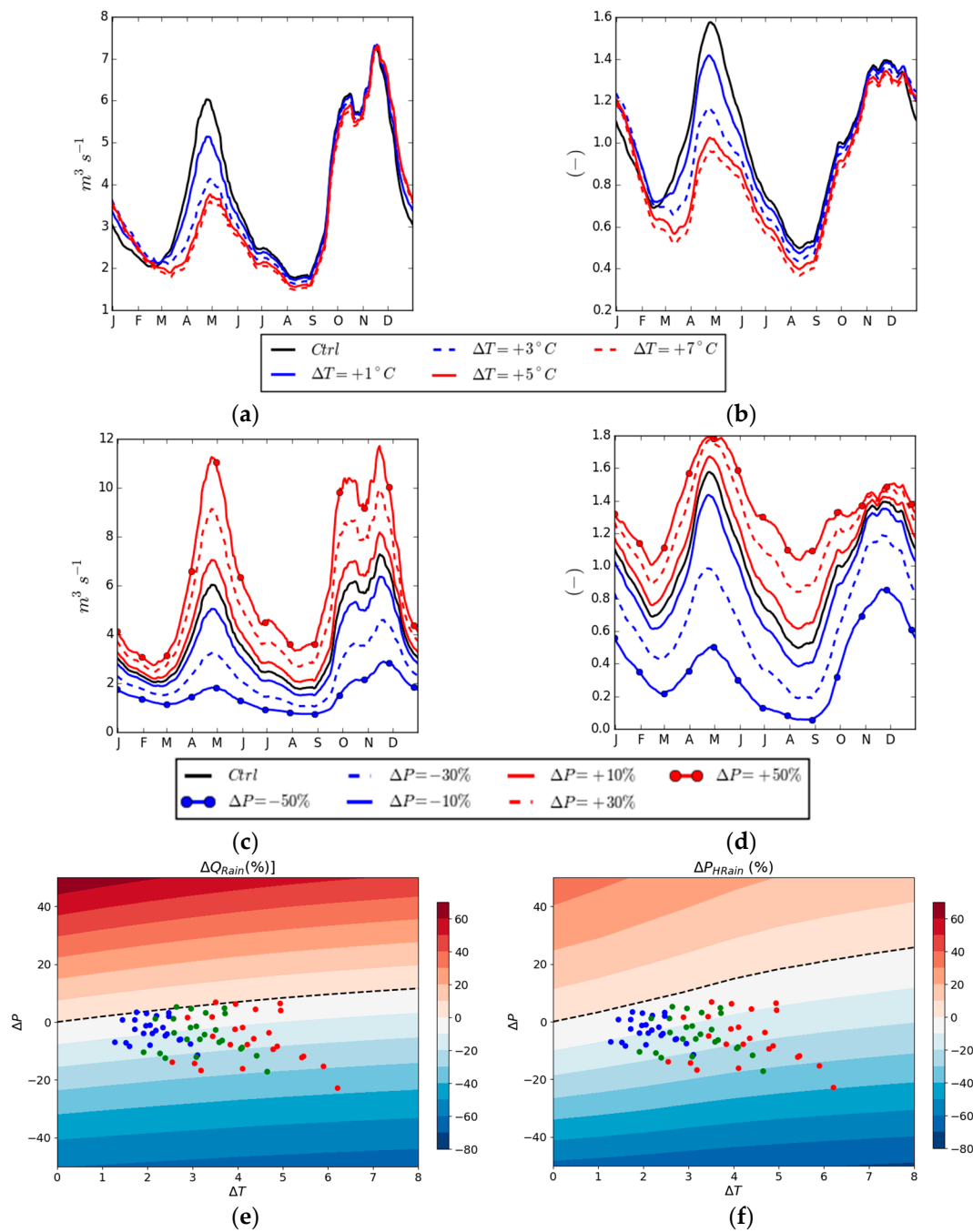


Figure 6. Average cycle of discharges (a,c) and RoR power generation (b,d) obtained for different temperature changes ΔT (a,b) or precipitation changes ΔP (c,d) over the Posina catchment. The cycles are smoothed over moving window of 30 days. RoR cycles were normalized regarding the generation obtained for the control climate. The climate response functions (e,f) respectively represent the changes (%) in average annual of discharge and RoR power generation. Dots show change factors for temperature and precipitation expected from CMIP5 experiments (see Figure 3 for details). The dashed black curve shows the ‘no change’ edge.

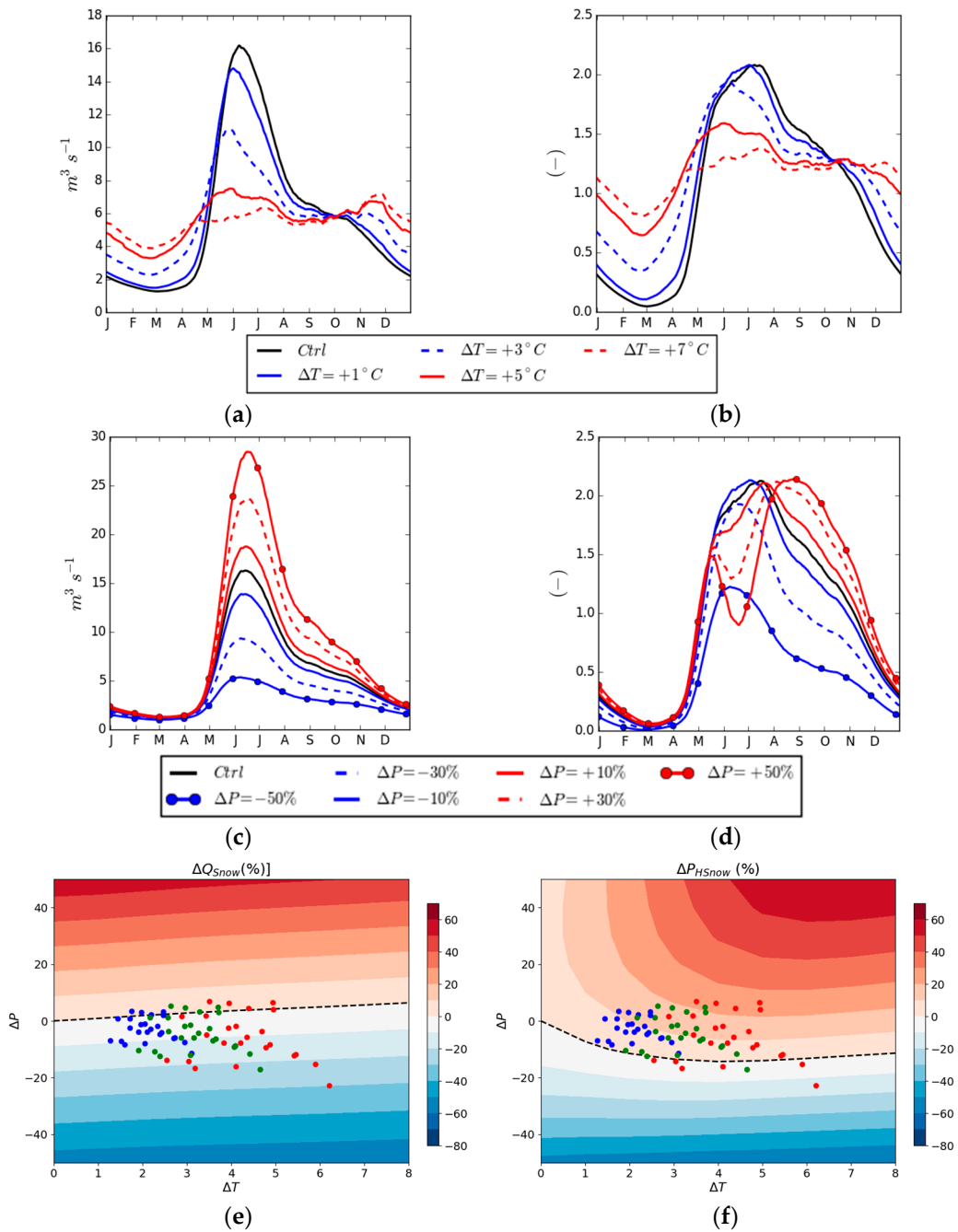


Figure 7. Same as Figure 6 for Cadipietra catchment.

Note that air temperature also influences solar PV generation (Equation (4)), although its effect is rather weak. For instance, when considering the extreme $+8^\circ C$ scenario, maximum daily solar PV generation decreases during very hot days by less than 5% while annual average generation only decreases by less than 3% (not shown).

The simulated energy load (Equation (1)) is impacted by temperature change only. Higher consumption during summer, with more use of cooling systems, and lower consumption during winter, with less use of heating systems, underpins the demand dependence to temperature illustrated on Figure 8. In the present case, decreasing winter consumption does not make up for increasing summer consumption. As a result, the average energy load slightly increases with temperature.

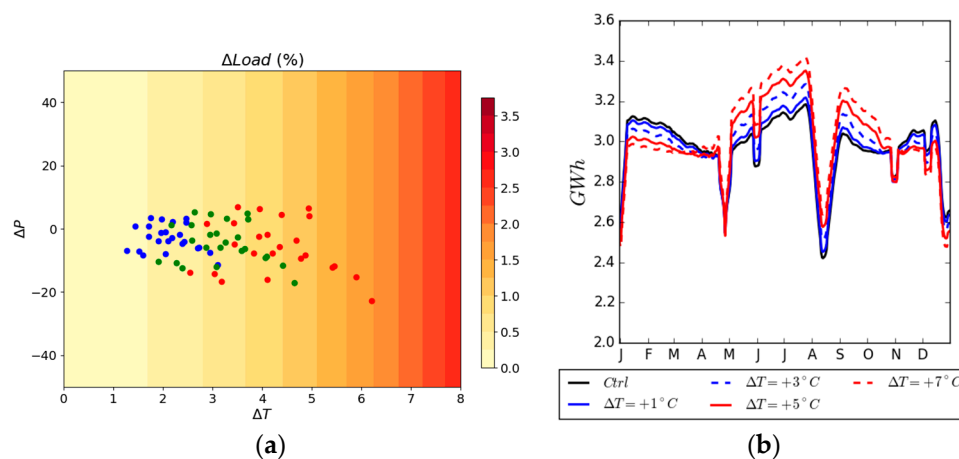


Figure 8. (a) Average daily load changes (%) from control period to future periods. Dots show expected temperature and precipitation changes as illustrated Figure 4. (b) Average inter-annual cycle of energy load obtained for control period and four temperature increase scenarios.

5.2. Future Penetration Rates

Figure 9 shows the CRF function of the regional penetration rate of the considered energy mix without any capacity. Due to the high share of RoR power coming from the Alpine area, this CRF shows a similar pattern than the ones obtained for $P_{H_{Snow}}$ (Figure 7f).

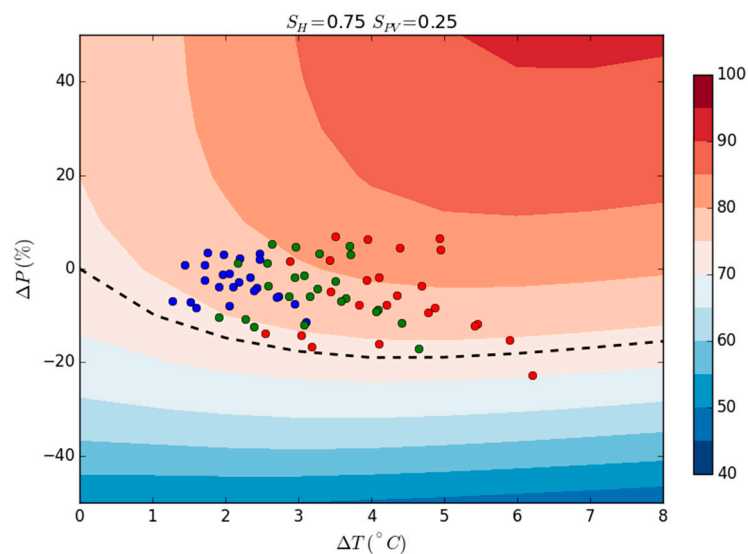


Figure 9. Climate Response Function of the penetration rate (%) when power generation comes from 25% of solar PV and 75% of RoR power (i.e., $S_{PV} = 0.25$). 75% of RoR power comes the alpine catchment (i.e., $S_H = 0.75$). Dots show the temperature and precipitation changes expected from CMIP5 experiments as illustrated on Figure 4. Dashed black line shows 'no penetration change' edge.

In a future climate, the main driver of the penetration rate is the change in precipitation. At a given level of temperature change, the sensitivity is higher for a decrease than for an increase in precipitation. For instance with no change in temperature, when precipitation changes by 40%, the penetration decreases by 15% for a precipitation decrease and increases by only 2.5% for a precipitation increase. As discussed previously for the influence on hydropower production, this might come from more frequent discharges exceeding the safety threshold Q_{max} . At a given level of either positive precipitation change or negative precipitation change by less than 12%, warmer conditions increase the penetration

rate under a twofold influence: the alpine RoR generation dominating the mix increases (cf. Section 5.1) and the RoR generation better matches the load in time.

A penetration rate is associated to each GCM experiment from its estimated changes in temperature and precipitation. We present Figure 10 the cumulative probability distribution function of the penetration rates for each future period. We note that almost all GCMs predict an increase of the penetration rate for all periods. Only one GCM predicts a decrease by about 2% over the 2080–2099 period. Although the dispersion of the penetration distribution increases with time, the mean ensemble rise by 4.3%, 5.4% and 5.7%, respectively for the period 2040–2059, 2060–2079 and 2080–2099.

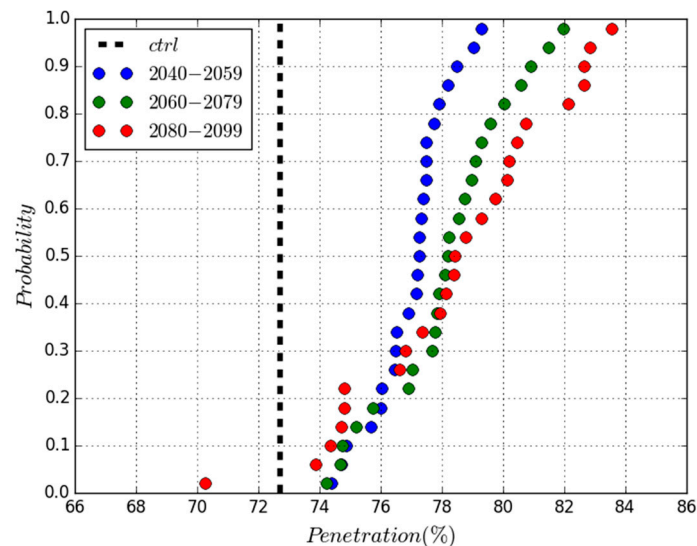


Figure 10. Cumulative distribution function (CDF) of penetration rate based on GCM projections (plotting position formula). The considered energy mix is defined by $S_{PV} = 0.25$ and $S_H = 0.75$. The dash line represents the penetration rate during the control period. Probabilities are computed using position-plotting formula by Hazen [60].

5.3. Future Penetration Rates with Storage

Figure 11 illustrates the evolution of the penetration rate for each energy source when considering a storage capacity. Note that the future penetration rate obtained for PV only account for the effect of temperature, assuming no change in solar radiation. Whatever the control or future period considered, increasing the storage capacity within the system logically increases the penetration rate of the VREs.

The changes in average temperature and precipitation have different impact on RoR penetration whether we look at either the lowland or the alpine catchment. For all storage capacities, the penetration rates decrease for the former and increase for the latter. We also note that the penetration rate distributions are much more spread for the lowland than for the alpine area because of the smoothing effect of the snowpack dynamic. The PV penetration rates do not significantly change, as expected from the minor role of the temperature in the power generation.

The penetration rates obtained for the considered mix are also presented Figure 11. For any storage capacity lower than one month of average load, the penetration rate in a future climate is expected to be roughly always greater than the one obtained during the control period. For instance, we note that the evolution of the penetration values obtained during the 2080–2099 period without storage corresponds to the penetration values obtained during the control period with one week of storage. These penetration rises follow from the fact that a system with low storage facility (i.e., less than one month) may take advantage of the increase in alpine RoR generation and of a better temporal match between generation and load. For systems with a large storage capacity (i.e., larger than one month), we observe for some GCMs a decrease in penetration from the 2040–2059 period to

the 2080–2099 period. Since these systems are designed to store the energy in excess and to release it when needed, such systems are less sensitive to the raw time generation-load mismatches. Conversely, they become more sensitive to the evolution of the mean generation.

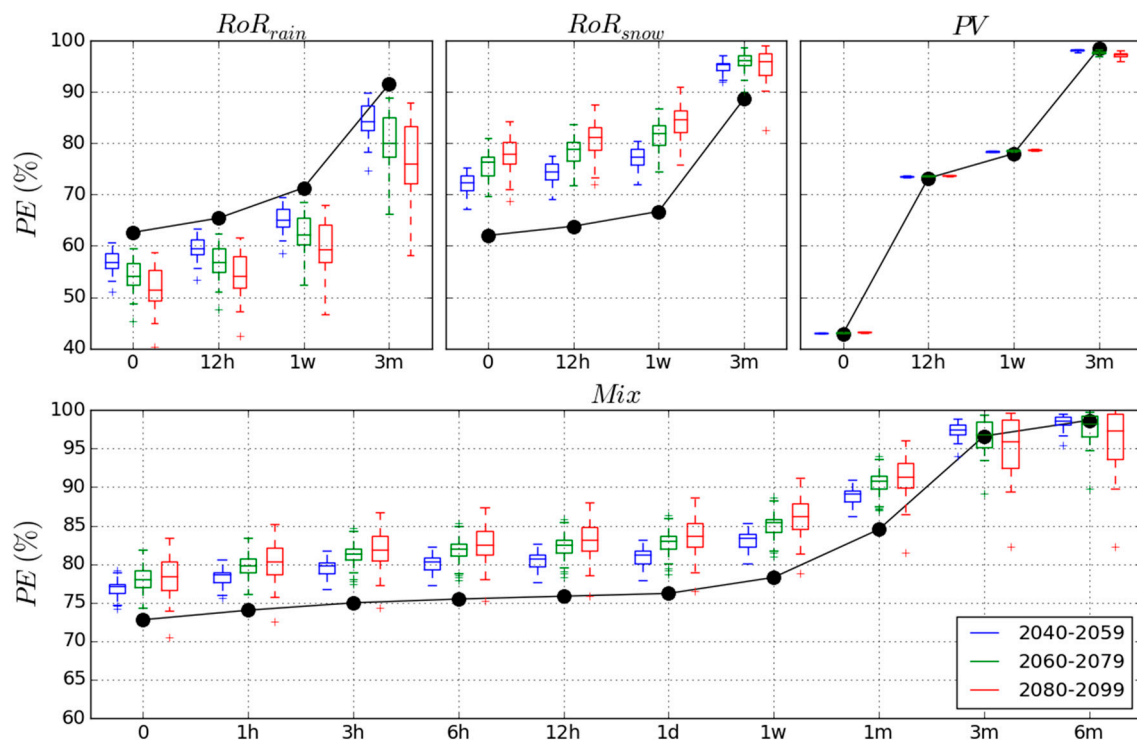


Figure 11. Evolution of the penetration rate as a function of GCM changes in precipitation and temperature variables for different storage capacities and for the given future periods. First row: from left to right, the penetration rates are given for RoR in low land area, RoR in alpine area, PV in the Veneto plains. Second row: penetration rate of the considered energy mix defined by $S_{PV} = 0.25$ and $S_H = 0.75$. Storage capacities are given in average load hours. Black dots show penetration rates obtained for the control period (same as Figure 5).

6. Discussion and Conclusions

In many places of the world, the on-going climate change is expected to modify VRE driving weather variables. In Northern Italy, an increase in average temperature is consistently predicted for the next decades. Mean precipitation is expected to slightly increase according to some GCMs but others predict a significant decrease in mean precipitation. Both changes are expected to affect VRE generation together with the electricity consumption in the region. As a result, the current regional energy balance between VRE generation and load is expected to change.

This study analyzed the evolution of the energy balance in Northern Italy via the penetration rate indicator defined as the percentage of supplied load over the considered period. We used the assumption that only solar- and hydro-power are used for supplying the load within the studied area. We focused on the most likely regional energy mix in the next decades, i.e., 25% of the generation coming from solar PV power and 75% of run-of-the river (RoR) hydropower. RoR power generation is shared between an alpine snow-dominated catchment and a lowland catchment (respectively 56% and 19% of the total generation). We applied the decision scaling approach, as developed by Brown et al. [19] for the assessment of the vulnerability of various water resource systems regarding climate change, to the analysis of the electricity system in Northern Italy.

In this region, results show non-linear changes of RoR power generation regarding expected changes in average precipitation and temperature, both in terms of average and seasonal organization.

According to the different hydro-meteorological processes involved in river flow generation, the climate change impacts vary from high to low altitudes. For the considered rain-fed catchment (i.e., low altitude), the decrease in average precipitation implies a decrease in RoR generation for all seasons. For snow dominated catchments (i.e., high altitude), the RoR generation is likely to increase although the discharges are expected to decrease. In this region, a decrease in average RoR generation is only observed if the average precipitation decreases by more than 12%. The seasonal organization of the RoR power generation within this area is also expected to be altered; lower generation is expected during spring and early summer while higher generation is expected in winter. Climate warming is expected to increase the annual electricity consumption with higher consumptions in summer (cooling) but lower consumptions in winter (heating).

Results show that without energy storage capacity, it is worth combining the considered energy sources since the related penetration is higher than the raw penetration obtained for each source individually. The penetration rate for a system with a low storage capacity (i.e., lower than one month of average load) is likely to increase in the next decade thanks to a modification in the temporal covariation structure between both production and load. For a system with a high storage capacity, the penetration rate is conversely expected to slightly decrease. With its ability to better exploit the yearly resource, such a system is indeed much more sensitive to changes in the mean resource.

This study considered a set of assumption and modelling choices that could be discussed or improved in further works. First, even though the simple change factor approach is very popular for testing system sensitivity to mean climate change, more sophisticated methods were recently developed. For instance, Steinschneider and Brown [61] developed a stochastic multisite weather generator able to account for possible changes in low-frequency variability. Using such a framework instead of the change factor method would allow the assessment of the role of change in time sequence frequency (e.g., what would be the impact of a long sequence of year with low/high VRE generation). This study analyses the impact of change in precipitation and temperatures only. Since the main driver of solar PV power is the radiation, further researches should also look at the effect of change in radiation time sequences.

Second, the electricity consumption is assumed to be only temperature dependent, although other climatic factors are well known for affecting the load (e.g., see [62] for the influence of humidity and cloud cover). Another limitation about the load model is that the simulated national electricity consumption is scaled according to the regional GDP. This neglects the differences in temporal pattern of the electricity consumption between the three considered provinces and the whole country; the latter being rather not informative because it averages consumption pattern from the North to South of the country. In other word, this means the parameters of the load model (Equation (1)) would take different values if regional values were used to calibrate the model. In fact, for the three considered provinces, higher (resp. lower) sensitivity of the electricity consumption to temperature in winter (resp. summer) is expected.

The use of statistics at the regional scale that could be obtained from Istat (<http://www.istat.it/en/>) and from Gestore Mercati Energetici (<http://www.mercatoelettrico.org>) could be integrated within a framework similar to the one described in [63] could be used to better define the regional consumption. However, the variability of the electricity consumption (in this case the seasonality) is known for being much lower than for the VRE generation (see for instance the power spectrum density on Figure 6 of the review by England et al. [2]). As such, a better description of the regional load should slightly influence the result of our study, but the general picture should hold.

The capacity to store the surplus of generation has been modeled with perfect efficiency that do not have real storage technologies such as batteries or pumped storage plants (for instance, the efficiency of a typical pumped storage plant is about 0.8). This is actually discussed in Ref [47]; the energy losses resulting from storage efficiencies lower than 1 can be compensated by oversizing the VRE generation (by using the scenario 120% scenario). However, the distribution of the total storage capacity into several storage technologies is a question per se that deserves to be address in further research works

by following a cost-benefit analysis framework, for instance. The levelized costs of VRE plants and storage facilities could be used to define the optimal combination of storage technologies but also the optimal average VRE generation (e.g., 100 or 120% scenario). Because of the aforementioned limitations, the simplified electricity system described in this study do not provide the literal portrayal of the real system. However, there is no doubt that the main results of this study that maps the effect of climate change on the complementarity between solar PV and RoR power in Northern Italy remain valid for the real system.

Acknowledgments: This work is part of the FP7 project COMPLEX (Knowledge based climate mitigation systems for a low carbon economy; Project FP7-ENV-2012 number: 308601; <http://owsgip.itc.utwente.nl/projects/complex/>). The authors would also like to thank two anonymous reviewers for helpful comments and suggestions.

Author Contributions: Baptiste François designed the methodology, carried out the power generation and electricity demand modeling, analyzed the results and wrote the article. Davide Zoccatelli carried out the hydrological modelling. Benoit Hingray carried out the climate change scenario modelling, and contributed to the results' analysis and composing the final text. Marco Borga, Casey Brown and Jean-Dominique Creutin contributed to the results' analysis and composing the final text. In addition, Jean-Dominique Creutin coordinated the project.

Conflicts of Interest: The authors declare no conflict of interest. The founding sponsors had no role in the design of the study; in the collection, analyses, or interpretation of data; in the writing of the manuscript, and in the decision to publish the results.

References

1. Jacobson, M.Z. Roadmaps to transition countries to 100% clean, renewable energy for all purposes to curtail global warming, Air Pollution, and Energy Risk. *Earth's Future* **2017**, *5*, 948–952. [CrossRef]
2. Engeland, K.; Borga, M.; Creutin, J.D.; François, B.; Ramos, M.H.; Vidal, J.P. Space-time variability of climate and hydro-meteorology and intermittent renewable energy production—A review. *Renew. Sustain. Energy Rev.* **2017**, *79*, 600–617. [CrossRef]
3. François, B.; Borga, M.; Anquetin, S.; Creutin, J.D.; Engeland, K.; Favre, A.C.; Hingray, B.; Ramos, M.H.; Raynaud, D.; Renard, B.; et al. Integrating hydropower and intermittent climate-related renewable energies: A call for hydrology. *Hydrol. Process* **2014**, *28*, 5465–5468. [CrossRef]
4. Saarinen, L.; Dahlbäck, N.; Lundin, U. Power system flexibility need induced by wind and solar power intermittency on time scales of 1–14 days. *Renew. Energy* **2015**, *83*, 339–344. [CrossRef]
5. Raunbak, M.; Zeyer, T.; Zhu, K.; Greiner, M. Principal Mismatch Patterns Across a Simplified Highly Renewable European Electricity Network. *Energies* **2017**, *10*, 1934. [CrossRef]
6. François, B. Influence of winter North-Atlantic Oscillation on Climate-Related-Energy penetration in Europe. *Renew. Energy* **2016**, *99*, 602–613. [CrossRef]
7. IEA. Energy and Climate Change: World Energy Outlook, Special Report. 2015. Available online: <https://www.iea.org> (accessed on 19 January 2018).
8. Jerez, S.; Tobin, I.; Vautard, R.; Montávez, J.P.; López-Romero, J.M.; Thais, F.; Bartok, B.; Christensen, O.B.; Colette, A.; Déqué, M.; et al. The impact of climate change on photovoltaic power generation in Europe. *Nat. Commun.* **2015**, *6*, 10014. [CrossRef] [PubMed]
9. Sullivan, P.; Colman, J.; Kalendra, E. *Predicting the Response of Electricity Load to Climate Change*; NREL Technical Report; National Renewable Energy Laboratory (NREL): Golden, CO, USA, 2015. Available online: <http://www.nrel.gov/docs/fy15osti/64297> (accessed on 19 January 2018).
10. Bridge, G.; Bouzarovski, S.; Bradshaw, M.; Eyre, N. Geographies of energy transition: Space, place and the low-carbon economy. *Energy Policy* **2013**, *53*, 331–340. [CrossRef]
11. Von Bremen, L. Large-scale variability of weather dependent renewable energy sources. In *Management of Weather and Climate Risk in the Energy Industry*; Springer: Berlin, Germany, 2010; pp. 189–206.
12. Becker, S.; Rodriguez, R.A.; Andresen, G.B.; Schramm, S.; Greiner, M. Transmission grid extensions during the build-up of a fully renewable pan-European electricity supply. *Energy* **2014**, *64*, 404–418. [CrossRef]
13. Wilby, R.L.; Dessai, S. Robust adaptation to climate change. *Weather* **2010**, *65*, 180–185. [CrossRef]

14. Tobin, I.; Vautard, R.; Balog, I.; Bréon, F.-M.; Jerez, S.; Ruti, P.M.; Thais, F.; Vrac, M.; Yiou, P. Assessing climate change impacts on European wind energy from ENSEMBLES high-resolution climate projections. *Clim. Chang.* **2015**, *128*, 99–112. [[CrossRef](#)]
15. Tobin, I.; Jerez, S.; Vautard, R.; Thais, F.; van Meijgaard, E.; Prein, A.; Déqué, M.; Kotlarski, S.; Maule, C.F.; Nikulin, G.; et al. Climate change impacts on the power generation potential of a European mid-century wind farms scenario. *Environ. Res. Lett.* **2016**, *11*, 034013. [[CrossRef](#)]
16. François, B.; Hingray, B.; Creutin, J.D.; Hendrickx, F. Estimating Water System Performance under Climate Change: Influence of the Management Strategy Modeling. *Water Resour. Manag.* **2015**, *29*, 4903–4918. [[CrossRef](#)]
17. Gaudard, L.; Gilli, M.; Romerio, F. Climate Change Impacts on Hydropower Management. *Water Resour. Manag.* **2013**, *27*, 5143–5156. [[CrossRef](#)]
18. Schaeffli, B. Projecting hydropower production under future climates: A guide for decision-makers and modelers to interpret and design climate change impact assessments. *Wiley Interdiscip. Rev. Water* **2015**, *2*, 271–289. [[CrossRef](#)]
19. Christensen, N.S.; Wood, A.W.; Voisin, N.; Lettenmaier, D.P.; Palmer, R.N. The Effects of Climate Change on the Hydrology and Water Resources of the Colorado River Basin. *Clim. Chang.* **2004**, *62*, 337–363. [[CrossRef](#)]
20. Brown, C.; Ghile, Y.; Laverty, M.; Li, K. Decision scaling: Linking bottom-up vulnerability analysis with climate projections in the water sector. *Water Resour. Res.* **2012**, *48*, W09537. [[CrossRef](#)]
21. Stainforth, D.A.; Downing, T.E.; Washington, R.; Lopez, A.; New, M. Issues in the interpretation of climate model ensembles to inform decisions. *Philos. Trans. R. Soc. Lond. A* **2007**, *365*, 2163–2177. [[CrossRef](#)] [[PubMed](#)]
22. Brown, C.; Wilby, R.L. An alternate approach to assessing climate risks. *Eos Trans. Am. Geophys. Union* **2012**, *93*, 401–402. [[CrossRef](#)]
23. Kundzewicz, Z.W.; Stakhiv, E.Z. Are climate models “ready for prime time” in water resources management applications, or is more research needed? *Hydrol. Sci. J.* **2010**, *55*, 1085–1089. [[CrossRef](#)]
24. Prudhomme, C.; Wilby, R.L.; Crooks, S.; Kay, A.; Reynard, N.S. Scenario-neutral approach to climate change impact studies: Application to flood risk. *J. Hydrol.* **2010**, *390*, 198–209. [[CrossRef](#)]
25. Poff, N.L.; Brown, C.M.; Grantham, T.E.; Matthews, J.H.; Palmer, M.A.; Spence, C.M.; Wilby, R.L.; Haasnoot, M.; Mendoza, G.F.; Dominique, K.C.; et al. Sustainable water management under future uncertainty with eco-engineering decision scaling. *Nat. Clim. Chang.* **2015**, *6*, 25–34. [[CrossRef](#)]
26. François, B.; Martino, S.; Tøfte, L.; Hingray, B.; Mo, B.; Creutin, J.-D. Effects of Increased Wind Power Generation on Mid-Norway’s Energy Balance under Climate Change: A Market Based Approach. *Energies* **2017**, *10*, 227. [[CrossRef](#)]
27. Norbiato, D.; Borga, M.; Dinale, R. Flash flood warning in ungauged basins by use of the flash flood guidance and model-based runoff thresholds. *Meteorol. Appl.* **2009**, *16*, 65–75. [[CrossRef](#)]
28. Gestore Servizi Energetici (GSE). *Statistical Report: Renewable Energy Power Plants in Italy*. Technical Report. 2011. Available online: <http://www.gse.it/it/> (accessed on 30 November 2014).
29. Moser, D.; Vettorato, D.; Vaccaro, R.; Del Buono, M.; Sparber, W. The PV Potential of South Tyrol: An Intelligent Use of Space. *Energy Procedia* **2014**, *57*, 1392–1400. [[CrossRef](#)]
30. François, B.; Borga, M.; Creutin, J.D.; Hingray, B.; Raynaud, D.; Sauterleute, J.F. Complementarity between Solar and Hydro Power: Sensitivity study to climate characteristics in Northern-Italy. *Renew. Energy* **2016**, *86*, 543–553. [[CrossRef](#)]
31. Hekkenberg, M.; Moll, H.C.; Uiterkamp, A.J.M.S. Dynamic temperature dependence patterns in future energy demand models in the context of climate change. *Energy* **2009**, *34*, 1797–1806. [[CrossRef](#)]
32. Psiloglou, B.E.; Giannakopoulos, C.; Majithia, S.; Petrakis, M. Factors affecting electricity demand in Athens, Greece and London, UK: A comparative assessment. *Energy* **2009**, *34*, 1855–1863. [[CrossRef](#)]
33. Nash, J.E.; Sutcliffe, J.V. River flow forecasting through conceptual models part I—A discussion of principles. *J. Hydrol.* **1970**, *10*, 282–290. [[CrossRef](#)]
34. Hänggi, P.; Weingartner, R. Variations in Discharge Volumes for Hydropower Generation in Switzerland. *Water Resour. Manag.* **2012**, *26*, 1231–1252. [[CrossRef](#)]
35. Norbiato, D.; Borga, M.; Degli Esposti, S.; Gaume, E.; Anquetin, S. Flash flood warning based on rainfall thresholds and soil moisture conditions: An assessment for gauged and ungauged basins. *J. Hydrol.* **2008**, *362*, 274–290. [[CrossRef](#)]

36. Norbiato, D.; Borga, M.; Merz, R.; Blöschl, G.; Carton, A. Controls on event runoff coefficients in the eastern Italian Alps. *J. Hydrol.* **2009**, *375*, 312–325. [[CrossRef](#)]
37. Cazorzi, F.; Dalla Fontana, G. Snowmelt modelling by combining air temperature and a distributed radiation index. *J. Hydrol.* **1996**, *181*, 169–187. [[CrossRef](#)]
38. Hargreaves, G.H.; Samani, Z.A. *Reference Crop Evapotranspiration from Ambient Air Temperature*; American Society of Agricultural Engineers: St. Joseph, MI, USA, 1985.
39. Moore, R. The PDM rainfall-runoff model. *Hydrol. Earth Syst. Sci.* **2007**, *11*, 483–499. [[CrossRef](#)]
40. Perpiñan, O.; Lorenzo, E.; Castro, M.A. On the calculation of energy produced by a PV grid-connected system. *Prog. Photovolt.* **2007**, *15*, 265–274. [[CrossRef](#)]
41. Duffie, J.A.; Beckman, W.A. *Solar Engineering of Thermal Processes*, 2nd ed.; Wiley: New York, NY, USA, 1991.
42. Jaramillo, O.A.; Borja, M.A.; Huacuz, J.M. Using hydropower to complement wind energy: A hybrid system to provide firm power. *Renew. Energy* **2004**, *29*, 1887–1909. [[CrossRef](#)]
43. François, B.; Hingray, B.; Raynaud, D.; Borga, M.; Creutin, J.D. Increasing climate-related-energy penetration by integrating run-of-the river hydropower to wind/solar mix. *Renew. Energy* **2016**, *87*, 686–696. [[CrossRef](#)]
44. François, B.; Zoccatelli, D.; Borga, M. Assessing small hydro/solar power complementarity in ungauged mountainous areas: A crash test study for hydrological prediction methods. *Energy* **2017**, *127*, 716–729. [[CrossRef](#)]
45. Ueckerdt, F.; Brecha, R.; Luderer, G. Analyzing major challenges of wind and solar variability in power systems. *Renew. Energy* **2015**, *81*, 1–10. [[CrossRef](#)]
46. Bett, P.E.; Thornton, H.E. The climatological relationships between wind and solar energy supply in Britain. *Renew. Energy* **2016**, *87*, 96–110. [[CrossRef](#)]
47. Heide, D.; von Bremen, L.; Greiner, M.; Hoffmann, C.; Speckmann, M.; Bofinger, S. Seasonal optimal mix of wind and solar power in a future, highly renewable Europe. *Renew. Energy* **2010**, *35*, 2483–2489. [[CrossRef](#)]
48. Heide, D.; Greiner, M.; von Bremen, L.; Hoffmann, C. Reduced storage and balancing needs in a fully renewable European power system with excess wind and solar power generation. *Renew. Energy* **2011**, *36*, 2515–2523. [[CrossRef](#)]
49. Chattopadhyay, K.; Kies, A.; Lorenz, E.; von Bremen, L.; Heinemann, D. The impact of different PV module configurations on storage and additional balancing needs for a fully renewable European power system. *Renew. Energy* **2017**, *113*, 176–189. [[CrossRef](#)]
50. Vautard, R.; Thais, F.; Tobin, I.; Bréon, F.-M.; de Lavergne, J.-G.D.; Colette, A.; Yiou, P.; Ruti, P.M. Regional climate model simulations indicate limited climatic impacts by operational and planned European wind farms. *Nat. Commun.* **2014**, *5*, 3196. [[CrossRef](#)] [[PubMed](#)]
51. Beaudin, M.; Zareipour, H.; Schellenberg, A.; Rosehart, W. Energy storage for mitigating the variability of renewable electricity sources: An updated review. *Energy Sustain. Dev.* **2010**, *14*, 302–314. [[CrossRef](#)]
52. Weitemeyer, S.; Kleinhans, D.; Vogt, T.; Agert, C. Integration of Renewable Energy Sources in future power systems: The role of storage. *Renew. Energy* **2015**, *75*, 14–20. [[CrossRef](#)]
53. Weitemeyer, S.; Kleinhans, D.; Wienholt, L.; Vogt, T.; Agert, C. A European Perspective: Potential of Grid and Storage for Balancing Renewable Power Systems. *Energy Technol.* **2015**, *4*, 114–122. [[CrossRef](#)]
54. Taylor, K.E.; Stouffer, R.J.; Meehl, G.A. An Overview of CMIP5 and the Experiment Design. *Bull. Am. Meteorol. Soc.* **2012**, *93*, 485–498. [[CrossRef](#)]
55. Hawkins, E.; Sutton, R. The potential to narrow uncertainty in projections of regional precipitation change. *Clim. Dyn.* **2011**, *37*, 407–418. [[CrossRef](#)]
56. Lafaysse, M.; Hingray, B.; Gailhard, J.; Mezghani, A.; Terray, L. Internal variability and model uncertainty components in a multireplicate multimodel ensemble of hydrometeorological projections. *Water Resour. Res.* **2014**, *50*, 3317–3341. [[CrossRef](#)]
57. Hingray, B.; Saïd, M. Partitioning internal variability and model uncertainty components in a multimodel multireplicate ensemble of climate projections. *J. Clim.* **2014**, *27*, 6779–6798. [[CrossRef](#)]
58. Knutti, R.; Masson, D.; Gettelman, A. Climate model genealogy: Generation CMIP5 and how we got there. *Geophys. Res. Lett.* **2013**, *40*, 1194–1199. [[CrossRef](#)]
59. Steinschneider, S.; McCrary, R.; Mearns, L.O.; Brown, C. The effects of climate model similarity on probabilistic climate projections and the implications for local, risk-based adaptation planning. *Geophys. Res. Lett.* **2015**, *42*, 5014–5044. [[CrossRef](#)]

60. Adeboye, O.B.; Alatise, M.O. Performance of probability distributions and plotting positions in estimating the flood of river Osun at Apoje Sub-basin, Nigeria. *Agric. Eng. Int. CIGR J.* **2007**, *9*, 1–21.
61. Steinschneider, S.; Brown, C. A semiparametric multivariate, multisite weather generator with low-frequency variability for use in climate risk assessments: Weather Generator for Climate Risk. *Water Resour. Res.* **2013**, *49*, 7205–7220. [[CrossRef](#)]
62. Apadula, F.; Bassini, A.; Elli, A.; Scapin, S. Relationships between meteorological variables and monthly electricity demand. *Appl. Energy* **2012**, *98*, 346–356. [[CrossRef](#)]
63. Scapin, S.; Apadula, F.; Brunetti, M.; Maugeri, M. High-resolution temperature fields to evaluate the response of Italian electricity demand to meteorological variables: An example of climate service for the energy sector. *Theor. Appl. Climatol.* **2016**, *125*, 729–742. [[CrossRef](#)]



© 2018 by the authors. Licensee MDPI, Basel, Switzerland. This article is an open access article distributed under the terms and conditions of the Creative Commons Attribution (CC BY) license (<http://creativecommons.org/licenses/by/4.0/>).